論文の内容の要旨

Atomistic Study on Deformation Mechanisms in Irradiated Zirconium Metal

(照射ジルコニウム金属の変形機構に関する原子論的研究)

劉 暁陽

1 Background and Objectives

Zirconium-based alloys are extensively used in light water reactor for fuel cladding materials, which form the primary containment barrier. During service in reactor, long term neutron irradiation induced pronounced hardening: a significant increase in yield stress and a strong reduction in strain hardening capacity. Increase in strength is usually attributed to the high density of small irradiation induced loops which act as obstacles against the dislocation gliding. Reduction in strain hardening capacity is related with dislocation channeling where irradiation induced defect clusters are overcome and then annihilated or dragged by dislocations under sufficient stress, these defect-free channels will therefore constitute preferred areas for further dislocation gliding, leading to plastic strain localization at the grain scale and causing the premature failure [1]. Recent statistical TEM observations indicate that dislocation channels mostly occurred in the basal planes [2]. However for HCP zirconium, the principle slip system is the prism plane before neutron irradiation. The underlying mechanisms for such changes in principle slip systems before and after neutron irradiation remain unsolved.

The objectives of this study are to analyze interaction between gliding dislocations and irradiation induced $\langle a \rangle$ type dislocation loops in zirconium in the atomistic level by means of molecular dynamics method, to determine roles of different slip systems (basal and prism) on localized deformation of irradiated zirconium, and then propose possible deformation mechanisms of irradiated zirconium under external shear deformation.

2 Simulation Methodologies

Fig.1 shows the simulation model. Two important slip systems are considered: prismatic and basal. For prismatic slip systems, the x axis is along the $[\bar{1}2\bar{1}0]$ crystallographic direction, y along $[\bar{1}010]$, and z along [0001]; for basal slip systems, the x axis is along the $[\bar{1}2\bar{1}0]$ crystallographic direction, y along [0001] , and z along $[10\bar{1}0]$. The Periodic boundary conditions are applied to x and z, constrained boundary conditions are applied to y. In the inner region **A** are the mobile atoms which are free to move along 3 dimensions during integration process, whereas atoms in the constrained regions **B** and **F** are fixed during integration process and can only adjust their positions along the loading direction when the external shear strain is applied.

The model is $32.3 \times 20.7 \times 22.4 nm$, containing 640,000 atoms. Loop density is a function of the simulation cell size and calculated to be $6.7 \times 10^{22}\ m^{-3}$. Dimensional quantities are made unitless in the range of -0.5 to 0.5.

One dislocation line and one dislocation loop are inserted into the model. The dislocation line is centered at

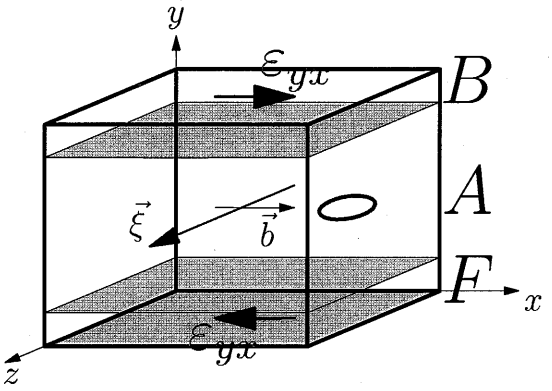

Figure 1: Schematic visualization of molecular dynamics simulation model

(-0.25 0 0) with line direction $\vec{\xi}$ along the z axis, Burgers vector $\vec{b}$ along the x axis and glide plane y=0. The irradiation induced dislocation loop is centered at (0.25 0 0) with varying Burgers vector, habit plane, nature (SIA or vacancy), position and size.

Four popular interatomic potentials for HCP zirconium metal are available in the open literature, Ackland1995[3] and Ackland2007 [4] are adopted in the molecular dynamics simulations.

Molecular dynamics simulations rely on the numerical integration of Newtron equation of motion for interesting atoms. The explicit time-reversible Velocity Verlet algorithm based on the Störmer-Verlet method[] is adopted. The NVT ensemble (constant number of atoms,volume and temperature) using a Nose-Hoover thermostat is adopted. Simulation temperature is kept at near 0K;

During deformation a resolved shear strain increment of 1×10^{-3} is applied to regions B and F in an opposite direction along x each step, and mobile atoms are relaxed until reaching equilibrium using the molecular dynamics method. The corresponding stress can be estimated from the internal force per unit area: $\sigma_{xy} = F_{INT}/A_{xz}$, where F_{INT} is defined as the total force from all the atoms in A and their images on all the atoms in B, A_{xz} is the area of the x-z cross-section of the inner region A.

Information on microstructure and motion of defect zones (including: dislocation, loop, defect clusters and so on) during interaction process is very important to understand the deformation mechanisms. Local energy filtering and local geometry approach are used to identify the location of defect zone. The successive three atom planes are highlighted with different colors, and projected in some direction to identify the microstructures of the defect zone. To obtain moving information of the dislocation line and dislocation loop, the relative displacements of interested

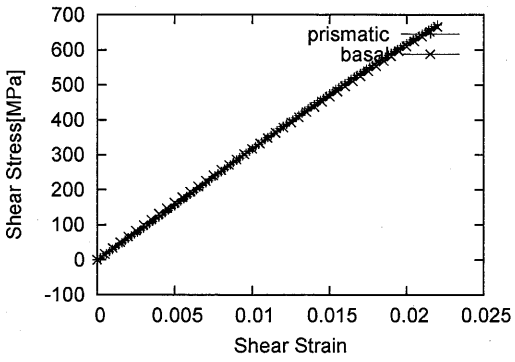

Figure 2: Strain-stress curve for the two crystals oriented for basal or prism glide

atoms for any two loading steps are calculated and plotted. In addition, an animation process is made to replay the interaction between gliding dislocation and dislocation loop.

3 Results and Discussion

3.1 Verification of the potential and code

One simple perfect model without either dislocation line or dislocation loop is built and relaxed to be equlilbrium. Based on the interatomic potential Ackland1995, cohesive energy is calculated to to be 6.243 eV, close to experimental value of 6.32 eV. Then shear deformation simulations for basal and prismatic slip systems are conducted, respectively. The shear stress-strain curve within elastic deformation range is plotted in Figure 2, the gradient of the shear stress-strain curve is equal to the corresponding shear modulus. The calculated shear modulus is in excellent agreement with the experimental values which further proves this package can calculate interatomic force correctly. it can be drawn that this simulation package is correct without bug.

3.2 Core structure of edge dislocation and dislocation loop

Three successive atom layers with red, white and dark from bottom to top respectively near y=0 are projected to the gliding plane to illustrate the core structure of the edge dislocation. Fig.3 shows the core structure of (a) the prismatic dislocation and (b)the basal dislocation respectively, the arrow shows the displacement direction of atoms in the top layer relative to those in the bottom layer. For prismatic dislocation, the displacements are along the $[\bar{1}2\bar{1}0]$ which is parallel to b. Evidently, it does not dissociating in the prismatic plane. The extent of the core structure is about $14b$. For the basal dislocation, the displacements are along the $[\bar{1}2\bar{1}0]$ and $[\bar{1}010]$, the basal dislocation splits into two Shockley partials in the basal plane, both of them have the screw component. The plane sequences in the regions I and III are dark...white...dark, corresponding to an perfect HCP structure, the plane sequences in the middle region II

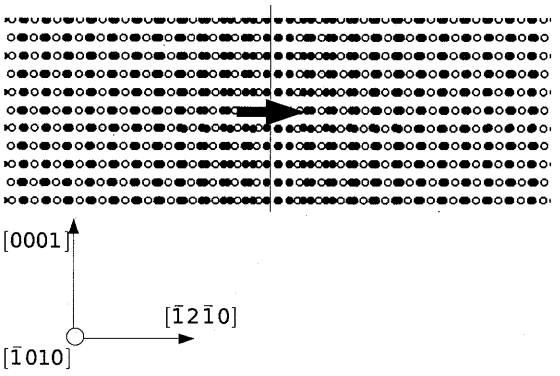

(a) prismatic dislocation

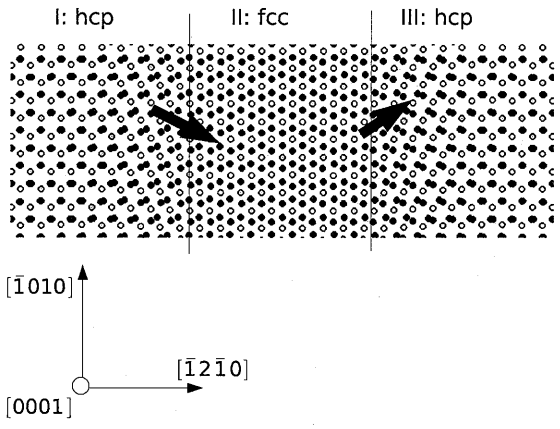

(b) basal dislocation

Figure 3: Relaxed core structure of the edge dislocation

are dark...white...red, means there is one intrinsic I_2 stacking fault with FCC structure, the width of the ribbon of the I_2 stacking fault is nearly $9b$. This dissociation process can be described by :

$$\frac{1}{3}[\bar{1}2\bar{1}0] \rightarrow \frac{1}{3}[01\bar{1}0] + \frac{1}{3}[\bar{1}100] \qquad (1)$$

The relaxed microstructures of two typical dislocation loops are shown as examples in fig.4 where the red atoms are of higher potential energy, Burger circuit is plotted. Fig.4(a) shows the (0001) atomic section of the cluster of 11 SIAs initially in $1/3[\bar{1}\bar{1}20]$ configuration, after $250ps$ of relaxation, the single SIAs are of the basal crowdion(BC) configuration, and all SIAs reside in the $\{\bar{1}010\}$ plane, the distortion of the cluster perimeter is not significant. According to the Burgers circuit analysis, the Burgers vector is along $1/3[\bar{1}\bar{1}20]$ with one 60° rotation away from the normal of its habit plane. Fig.4(b) shows the (0001) atomic plane of the cluster of 49 vacancies initially in the $\{01\bar{1}0\}$ plane, after $250ps$ of relaxation, these vacancies reside in the $\{01\bar{1}0\}$ plane with the Burgers vector $1/3[\bar{1}2\bar{1}0]$. These results are compatible with the experiment observations[5].

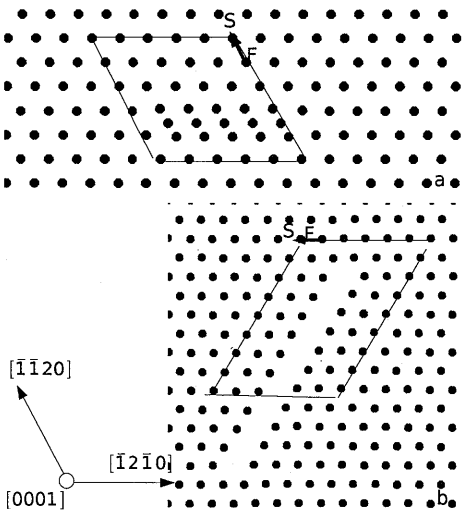

Figure 4: Relaxed configuration of (a) the 11 SIAs cluster initially in $1/3[\bar{1}\bar{1}20]$ configuration and (b) the 49 vacancies cluster initially in $1/3[\bar{1}2\bar{1}0]$ configuration

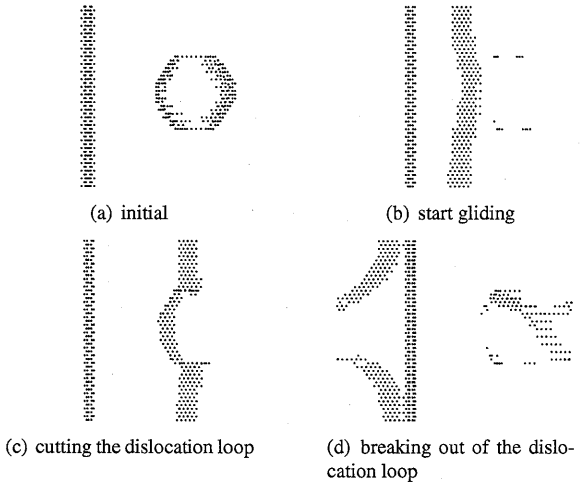

Figure 5: Interaction between $\langle a_1 \rangle$ edge dislocation and $\langle a_2 \rangle$ vacancy loop: Y projection of atoms in x-z planes near y=0

3.3 Interaction between $\langle a_1 \rangle$ edge prismatic dislocation and $\langle a_2 \rangle$ vacancy loop

The interaction between one prismatic dislocation and $\langle a_2 \rangle$ clusters of 49 vacancies is calculated. Figure 5 shows the 2-dimensional snapshots of different interaction stages, respectively. Red atoms represent they are near the defect zone with high potential energy. Figure 5(a) shows the initial structure before deformation. The dislocation is along the z in the gliding plane y=0, with Burgers vector $\langle a_1 \rangle$, and the dislocation loop habits in the $\{a_1\}$ plane with Burgers vector $\langle a_2 \rangle$. The poles of the dislocation loop along the dislocation line z are interacting with the the basal plane, and dissociate into two Shockley partials. Figure 5(b) shows the dislocation line has start gliding. It will leave one row of vacancies at its original position which are sessile. Due to the attraction from the vacancy dislocation loop, dislocation line bend towards it. Under external shear stress, the dislocation loop also moves, the left parts are moving along the $\langle -a_2 \rangle$ whereas the right parts are moving along the $\langle a_2 \rangle$, changing the loop shape. The left parts move a little slowly than the right parts. Figure 5(c) shows the dislocation line is interacting the dislocation loop. Because the shape of the dislocation loop is changed so that most of the dislocation loop are not in the same plane as the gliding plane of the dislocation, then the dislocation does not interact with the dislocation loop, except of two poles of dislocation loop along the dislocation line z. Therefore the segments of the dislocation line far away from the dislocation loop can continue to move easily whereas the segments near the dislocation loop bows out strongly because they are pinned by that two poles of the dislocation loop. Figure 5(d) shows the dislocation line is breaking out of the dislocation loop and continues to glide.

In addition, the z projection of interaction between different dislocation segment and dislocation loop, it is clarified that the segments near the dislocation loop glide in the different plane whereas the segments far away from the dislocation loop always glide in the same plane, there must be one junction between these two segments which can not glide in the gliding plane. Such junctions make it difficult for the dislocation line to break out of the dislocation loop.

3.4 Interaction between $\langle a_1 \rangle$ edge dislocation and $\langle a_1 \rangle$ SIA loop

The interaction of one basal edge dislocation line and one $\langle a_1 \rangle$ cluster of 11 SIAs is calculated. Figure 6 shows the Y projection of atoms in the x-z planes near y=0 at different deformation stages, under such view, the section is the basal plane, atoms are plotted in red, black and white depending on their potential energy form high to cohesive energy. Figure 6(a) shows the structure of dislocation line and dislocation loop at the initial stage when there is no external stress. The edge dislocation line dissociates into two Shockley partials in the basal plane between them the stacking fault forms with FCC structure. The width of the stacking fault is about $15b$. Two segments of dislocation loop intersecting with basal plane are calculated by drawing Burgers circuit. The SIAs is in the crowdion position along Burgers vector $\langle a_1 \rangle$ and habit in the $\{a_3\}$ plane. Fig-

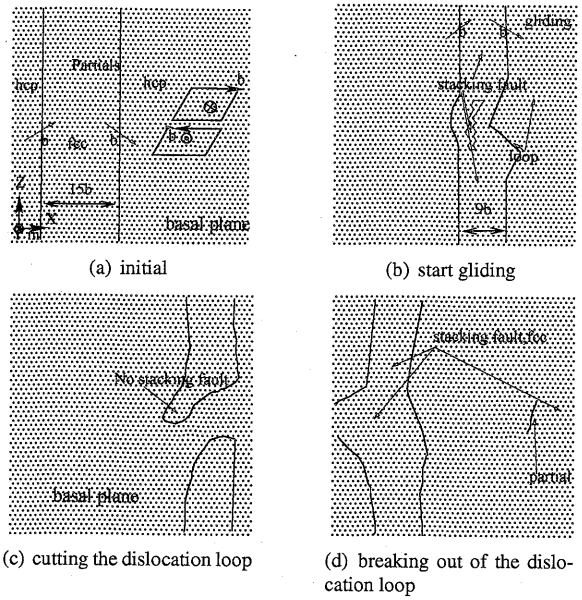

(a) initial (b) start gliding

(c) cutting the dislocation loop (d) breaking out of the dislocation loop

Figure 6: Interaction between $\langle a_1 \rangle$ edge dislocation and $\langle a_1 \rangle$ SIA loop: Y projection of atoms in x-z planes near y=0

ure 6(b) shows the microstructure of dislocation line and dislocation loop under shear strain 2.0%. Under external shear stress, partials leave from original position and are moving toward the dislocation loop. The leading partial bows out strongly due to the repulsion from SIA dislocation loop, the trailing partial moves a little faster than the leading one which makes the stacking fault zone narrowed, for example, the segment near the dislocation loop are narrowed to be $1b$, whereas the segments far away from the dislocation loop to be $9b$. Figure 6(c) shows the structure of dislocation line and dislocation loop under shear strain 8.0%. Segments of partials far away from the dislocation loop may continue to gliding, the dislocation loop has little effect on the gliding of them. Segments of partials near the dislocation loop are cutting the dislocation loop, due to the strong repulsion from the SIA dislocation loop and the moving forward trailing partials, the stacking fault between these two partials becomes narrowed and is lock by the dislocation loop. Figure 6(d) shows the structure of dislocation line and dislocation loop under shear strain 10.0%. With increasing shear strain, locked part of partials are released from the SIA dislocation loop, the leading partial can continue to glide as before interaction. The trailing partial bows out by the attraction from SIA dislocation loop, but will continue to glide as before interaction.

According to Saada and Wshburn process[6], when a a_1 dislocation gliding in the basal plane interacts with a a_1 loop, kinks are produced during interaction processes. Because the kinks are in the same plane as the dislocation line, they have no special effects on the dislocation gliding.

4 Conclusions

This study is the first molecular dynamics simulation concerning dislocation deformation mechanism in irradiated HCP zirconium. The primary simulation findings are summarized as following:

- Edge dislocation dissociates into two Shockley partials in the basal plane, however it does not dissociate in the prismatic plane;
- The dislocation slipping between planes with wide distance may contribute to plastic deformation and is considered to be physically reasonable.
- Two versions of interatomic potential Ackland1995 and Ackland2007 are compared in the MD simulation, only the latter can give correct stacking fault in the basal and prism plane.
- For interactions between $\langle a_1 \rangle$ prismatic edge dislocation and $\langle a_1 \rangle$ dislocation loop, kinks are produced during interaction processes. The dislocation line glides in the same plane as before interaction. The junctions are glissile.
- For interactions between $\langle a_1 \rangle$ prismatic edge dislocation and $\langle a_{2|3} \rangle$ dislocation loop, jogs are produced during interaction processes. Segments of the dislocation line cutting through the center of the dislocation loop glide in the different plane with those of far away from the dislocation loop. The junctions are sessile.
- For interactions between $\langle a_1 \rangle$ basal edge dislocation and $\langle a_{1|2|3} \rangle$ dislocation loop, kinks always are produced during interaction processes. The dislocation line glides in the same plane as before interaction. The junctions are glissile.

Based on the simulation results, dislocation breaking ability is proposed to determine how easily it is for the dislocation to break out of the dislocation loop and subsequently form the dislocation channeling. Two cases over three in the prismatic plane are of lower dislocation breaking ability, in contrast all cases in the basal plane are of hinger dislocation breaking ability. Such differences are attributed to the productions of interactions between dislocation line and dislocation loop, and lead to low possibility of dislocation channelings in the prismatic planes. These results are in good agreement with TEM observations of dislocation channels in the irradiated Zircaloy.

References

[1] M.Griffiths, ASTM STP 1295 (1996) 580.

[2] F.Onimus, I.Monnet, J.L.Bechade, C.Prioul, P.Pilvin, J.Nucl.Mater. 328 (2004) 165.

[3] G.J.Ackland, S.J.Wooding, D.J.Bacon, Phil.Mag.A 71 (1995) 553.

[4] M.I.Mendelev, G.J.Ackland, Phil.Mag.Let. 87 (2007) 5.

[5] Radiation Damage of Structure Materials, Elsevier, 1994.

[6] P.B.Hirsch, Proceedings of a conference on point defect behavior and diffusional processes, 1976, p. 13.